Nanoscale patterning of chemical order induced by displacement cascades in irradiated alloys. I. A kinetic Monte Carlo study

Jia Ye and Pascal Bellon*
Department of Materials Science and Engineering, University of Illinois at Urbana-Champaign, Illinois 61801, USA
(Received 19 February 2004; published 8 September 2004)

Dense displacement cascades produced by irradiation with energetic particles lead to the formation of disordered zones in chemically ordered alloys. At temperatures below the order-disorder transition, these disordered zones, whose sizes range from a few to several nanometers, are annealed out by thermally activated atomic migration. Under sustained irradiation, the competition between these two dynamics may drive the system into various steady states of order. Kinetic Monte Carlo simulations are employed to identify these steady states in a model binary alloy that forms an $L1_2$ ordered phase at equilibrium. Besides the expected long-range ordered and disordered steady states, a new state is observed, where the microstructure is comprised of well-ordered domains of finite size. This steady-state patterning of order is identified by direct visualizations of the configurations, and by using an effective fluctuation-dissipation formula to analyze the behavior of the fluctuations of order upon approaching the long-range ordered steady state. It is shown that the patterning state becomes stable only when the disordered zones exceed a threshold size. Above this threshold size, reordering of cascade-induced disordered zones proceeds in two stages: new antiphase domains form first, and then shrink to the benefit of the matrix. This two-stage reordering is at the origin of the dynamical stabilization of patterns of order. The present results, which indicate that ion-beam processing could be used to synthesize ordered nanocomposites with tunable sizes, call for specific experimental tests.

DOI: 10.1103/PhysRevB.70.094104 PACS number(s): 61.80.Az, 05.70.Ln, 47.54.+r, 64.60.Cn

I. INTRODUCTION

Materials irradiated with energetic particles are dissipative systems since energy continuously flows from the environment into these materials.[1] Under appropriate external forcing, dissipative systems display the remarkable ability to self-organize into patterns.[2,3] In the case of irradiated materials, patterns of structural defects, such as voids, bubbles, dislocation loops, and stacking fault tetrahedra, have been observed and modeled in the past three decades.[4,5] In most cases, a necessary condition for pattern formation is that irradiation leads to the formation of dense displacement cascades. These displacement cascades induce an asymmetry in the production of clustered vacancies and interstitials, and this asymmetry plays a fundamental role in the onset of patterning.[5]

Displacement cascades are also remarkable in the sense that they introduce at least two new length scales in the description of irradiated materials. Indeed, a cascade extends over a distance L, and atoms in this cascade undergo forced relocations following a distribution that possesses a characteristic relocation distance, R. We have shown that the existence of this relocation range, and the resulting finite-range atomic mixing, introduce a nonlocal term in the kinetic equation that describes the evolution of the composition field.[6] In the case of an alloy system that would decompose into two phases at equilibrium, the competition between short-range thermally activated decomposition and finite-range forced mixing can lead to the dynamical stabilization of compositional patterns. These patterns form only when R exceeds a critical value R_c, and the maximum characteristic scale of the patterns is bounded by $4\pi R_c$. In the present work we employ kinetic Monte Carlo simulations to demonstrate that the cascade size, L, can lead to similar patterning reaction, albeit for the degree of chemical order. In a companion paper, we introduce an analytical model to study this patterning of chemical order.[7]

Let us first recall some important characteristics of the disordered zones created by displacement cascades in ordered alloys. These zones have been studied experimentally using superlattice reflections to form dark-field transmission electron microscopy (DF-TEM) images. Results have been reported for several alloys (see Ref. 8 for a review), including Cu_3Au,[9–11] Ni_3Al,[11] Zr_3Al,[12] which all form an $L1_2$ ordered structure, on Cu_3Pd,[13] which forms a $D0_{22}$ ordered structure, and Fe_3Al,[13] which forms a $D0_3$ ordered phase. The aspect ratio and size distribution of the disordered zones, which appear as dark regions in superlattice DF-TEM images, have been studied as a function of the mass and the energy of the projectile, and as a function of the irradiation temperature. Average diameters range from 3 to 10 nm in Cu_3Au,[8,10] and from 5 to 9 nm for Ni_3Al.[11] As the projectile energy increases, the size of the disordered zones saturates because of the formation of subcascades. It is difficult, from these experimental results, to quantify the amount of chemical disorder achieved in the zones. Molecular dynamics (MD) simulations, which have been extensively used to analyze disordered zones produced by dense displacement cascades,[14–19] provide a direct measure of this disordering, although the interatomic potentials used in the simulations may affect the results somewhat. Nevertheless, in all studies of cascades initiated with primary knock-on atom (PKA) energies exceeding 1 keV, there is a well-defined zone where the long-range order (LRO) parameter is essentially zero.[14] The extension of these zones, which will be identified as the disordered zones in the remaining of the article, coincide

reasonably well with the experimental values given above. We note that the disordered zones may display some short-range order (SRO).[14,15] The degree of SRO is often found to increase from a low value at the center to a moderate or high value near the periphery of the disordered zone. This short-range order is more pronounced in cascades initiated in Ni_3Al than in Cu_3Au, most likely because of the larger mixing forced by the cascade in Cu_3Au and because of the lower ordering energy in this alloy.[15]

The goal of the present work is to study the long-time evolution of an ordered alloy undergoing sustained irradiation, under irradiation conditions that produce disordered zones. The kinetic Monte Carlo (KMC) technique makes it possible to simulate such an alloy over long physical times, unlike MD, while retaining the full information on temporal and spatial atomic correlations, unlike phase field models. While KMC simulations have been used previously to study the dissolution of ordered precipitates in the presence of cascades[20] and the reordering kinetics after the introduction of disordered zones,[21] we are not aware of any study concerned with the long-time microstructures resulting from the dynamical competition between irradiation-induced cascade disordering and thermally activated reordering. In Sec. II, we present the model $L1_2$ alloy selected for the simulations, as well as the details of the KMC simulations. Results obtained upon varying the rate of introduction of the disordered zones and the cascade size are given in Sec. III for stoichiometric alloys, and in Sec. IV for nonstoichiometric alloys. These results are then discussed in Sec. V.

II. KINETIC MONTE CARLO SIMULATIONS

The $A_{1-cB}B_{cB}$ model alloy selected for the present study has been previously investigated by Abinandanan *et al.*[22] The thermodynamics and the kinetics of this alloy, which undergoes $L1_2$ ordering, are already well characterized.[22] The equilibrium phase diagram is identical to the one given in Fig. 3 in Ref. 22. In this model, A and B atoms interact by first and second nearest-neighbor pair interactions $\varepsilon_{ij}^{(k)}$ ($k=1,2$ and $i,j=A,B$). The ordering energies' first and second nearest neighbors are $V_1=2\varepsilon_{AB}^{(1)}-\varepsilon_{AA}^{(1)}-\varepsilon_{BB}^{(1)}=-0.160$ eV and $V_2=2\varepsilon_{AB}^{(2)}-\varepsilon_{AA}^{(2)}-\varepsilon_{BB}^{(2)}=0.064$ eV. These parameters are such that the phase diagram closely resembles that of Ni–Al for Ni-rich compositions. The use of a nonzero V_2 also overcomes the problem met when only first nearest-neighbor interactions are used, which results in the existence of zero-energy antiphase boundaries (APBs) between the four translation variants of the $L1_2$ structure.[23] At the $L1_2$ stoichiometric composition, $c_B=0.25$, the $A1-L1_2$ order-disorder transition occurs at a temperature $T=0.155$ eV. Unless stated otherwise, all simulations are performed at T $=0.09$ eV and for $c_B=0.25$. At this temperature, the $A1-L1_2$ two-phase domain extends from $c_B\approx0.10$ to $c_B\approx0.20$.

The simulations are based on a kinetic model where atom migration can proceed by two processes acting in parallel, the thermally activated migration of vacancies and the forced exchanges of nearest-neighbor atoms in displacement cascades. A detailed description of the model used for thermal diffusion can be found in Refs. 22 and 24. The A and B atoms occupy sites on a rigid face-centered cubic (fcc) lattice containing $L\times L\times L$ sites, with $L=64$ or 128, and with periodic boundary conditions. A single vacancy is placed in the system, and the frequency of atom-vacancy exchange is determined using standard rate theory. The activation energy is given by the energy required to break the bonds between the jumping atom and its surrounding, less the energy recovered when the atom is placed at the saddle-point position. The vacancy migrates with an attempt frequency $\nu_0=10^{14}$ s^{-1}, and the average of migration energies in pure elements is arbitrarily set at $E_{m,v}=0.8$ eV. This value is used to determine the contribution of the migrating atom to the saddle-point energy, and it thus sets the time scale for thermal migration. Unless stated otherwise, simulations are carried out with a lattice size $L=64$. When $L=128$ is used to check finite-size effects, the cascade frequency is rescaled to account for the change in vacancy concentration with the system size.[25]

The forced mixing and disordering produced by displacement cascades is introduced by forcing exchanges of atoms in the cascade. In the present model, four parameters are used to specify this forced mixing. The first parameter is the rate of introduction of cascade per atom, Γ_c. Three parameters are then used to characterize a cascade: the spatial extension of the cascade, the relocation distance of atoms in the cascade, and the fraction of atoms undergoing exchanges in the cascade, which is referred to as the cascade density. For simplicity, the volume of the cascade is assumed to be spherical, and only one cascade size is used during each KMC run. These simplifications do not affect the generality of the results. The cascade density has been set to 80% in this work, unless specified otherwise, to produce zones where the degree of LRO is near zero when cascades are initiated in a perfectly ordered matrix. We will show, however, that a 50% cascade density, which retains about half of the long-range order parameter of the matrix, leads to significantly different results. In the following, we characterize the cascade size by the number of forced pair exchanges in one cascade, b. For example, for a spherical cascade containing 10 000 atoms, using an 80% density, 8000 distinct atoms, e.g., $b=4000$ atom pairs, are exchanged at once. The cascade size is varied from $b=1$, which in fact corresponds to irradiation without cascade, to $b=4002$, which corresponds to a cascade diameter of ≈6 nm in Ni_3Al. As for the relocation range, forced exchanges are performed between nearest-neighbor atoms, in order to prevent this parameter from inducing compositional patterns. The short range used here for forced exchanges is indeed below the critical value for producing such patterns.[26,27] Finally, it is useful to introduce the ballistic jump frequency, $\Gamma_b=b\times\Gamma_c$, which is a measure of the disordering rate. In the radiation damage community, $2\Gamma_b$ is referred to as the number of replacements par atom per second.[1] The present kinetic model does not include interstitials, sources and sinks for point defects, and elastic effects. The possible role played by these effects is discussed in Sec. IV.

The time evolution of the system is built using a residence-time algorithm,[22,24] where the frequency of vacancy exchanges is weighted against the frequency of cas-

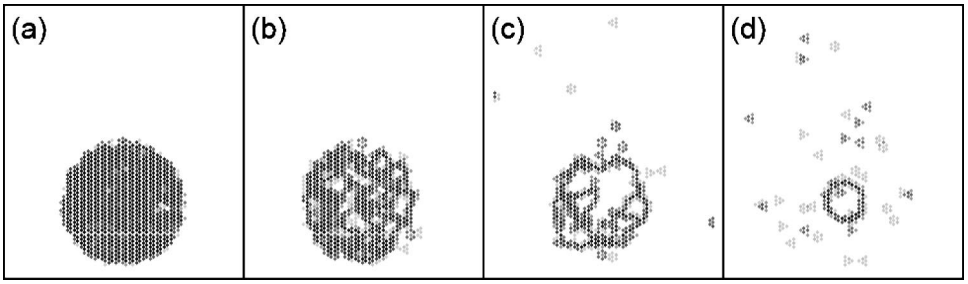

FIG. 1. {111} maps of the local degree of order $\eta(\mathbf{r})$ of instantaneous configurations after the introduction of one large dense cascade ($b=8000$, density$=80\%$, $T=0.09$ eV, system size 64^3): (a) $t=0$ s; (b) $t=0.0038$ s; (c) $t=0.0232$ s; (d) $t=0.0861$ s. White corresponds to fully ordered and black to fully disordered sites.

cade formation. One of the two kinds of events is randomly chosen according to their relative probabilities, and time is updated as the inverse of the sum of the individual frequencies.

Simulation results are analyzed using complementary methods, encompassing direct visualization of the configurations, determination of the size and number of ordered clusters belonging to any variant, and calculation of the spherically averaged structure factor, centered either on a Bragg peak or on an $L1_2$ superlattice position.[27] For direct visualization of the configurations, a local degree of order, $\eta(\mathbf{r}_i)$, is defined as $\eta(\mathbf{r}_i)=(1-c_B)^2(\alpha_2-\alpha_1)^2$, where α_1 and α_2 are the first and second nearest-neighbor Warren-Cowley short-range order parameters around a central site at $\mathbf{r}_i$, respectively.[28] It is easy to check that $\eta(\mathbf{r}_i)$ ranges from 0 for a random local environment to 1 for a perfect $L1_2$ environment. An alternative way of visualizing the ordered regions, which also makes it possible to identify the four variants of the $L1_2$ ordered structure, is to display only B atoms, using four colors (or four different symbols), one for each simple cubic sublattice a B atom may belong to. A global degree of order of a configuration, η, is measured by taking the square root of the average structure factor integrated from $0.8\mathbf{k}_s$ to $1.2\mathbf{k}_s$, where $\mathbf{k}_s=\{100\}$ is the $\mathbf{k}$ vector of the superlattice reflections, and by normalizing this value so that $\eta=1$ corresponds to a perfectly long-range ordered stoichiometric alloy. Before integrating the structure factor, a background intensity is subtracted.[23] η, which is mostly a measure of the degree of LRO, may include some contribution from the SRO. However, as discussed in Sec. III C, the relative LRO-to-SRO contribution scales with the diffracting volume raised to the power one-half; the contribution of the SRO can thus be quantified, and reduced, by increasing the simulation cell size.

III. KMC RESULTS AND ANALYSIS FOR STOICHIOMETRIC ALLOY

In this section we present the simulation results obtained for stoichiometric composition $c_B=0.25$. We start by following the thermal recovery process after one large cascade is initiated in an initially long-range ordered alloy. We then identify three steady states that are stable under sustained irradiation with dense cascades. Finally, we construct a dynamical phase diagram that yields the domain of stability of these steady states.

A. Reordering after one cascade

Figure 1 shows the evolution of an initially perfectly long-range ordered alloy after one large and dense cascade ($b=8000$, density$=80\%$). As the simulation is performed at $T=0.09$ eV, a temperature below the critical temperature, the disordered zone is annealed out by the migration of the vacancy. Direct visualization of the configurations reveals the existence of two distinct stages. In the first stage, the disordered zone reorders into small clusters that belong to the four variants available in an $L1_2$ structure. The presence of domains belonging to the four variants is also confirmed by displaying B atoms with four colors, one for each simple cubic sublattice (see Fig. 1 in Ref. 29). In the second stage, these small-ordered domains shrink and disappear by motion of antiphase boundaries, to the benefit of the matrix. These two stages are clearly identified by measuring the number of B atoms that belong either to the matrix or to small ordered clusters (see Fig. 2 in Ref. 29). This plot also reveals that the two stages overlap. Once the first stage is over, here after ≈ 0.0038 s, the radius of the reordered zone shrinks with time as $t^{1/2}$ (see Fig. 3 in Ref. 29), in agreement with the Allen-Cahn theory.[30]

Even though we are interested in dense cascades in this work, we stress that when the cascade is dilute, typically for a fraction of exchanged atoms of 50% or less, the relaxation of the system is very different. For such dilute cascades (see Fig. 4 in Ref. 29), the reordering does not lead to the formation of antiphase domains. Instead, the cascade zone is cut into several small and irregular disordered zones. These zones reorder directly by the inward migration of their boundary with the ordered matrix, and no new domains are created.

We now return to the case of dense cascades. Antiphase domains appear only when the cascade size is large enough for them to form during the migration of the vacancy within the disordered zone. For the generic parameters used in our simulations, this minimum cascade size is around $b=100$. Under sustained irradiation conditions, one anticipates that, if the average time between two cascades is shorter than the time required to fully anneal the previous cascade ($t\approx 0.1$ s here), but longer than the time necessary to reorder the dis-

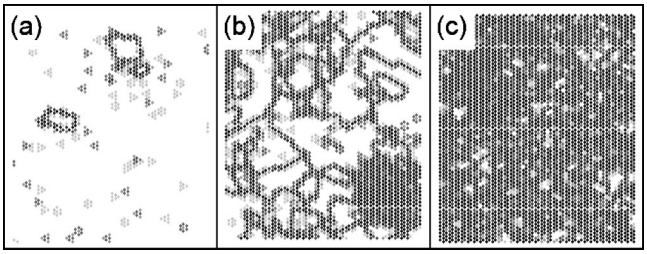

FIG. 2. {111} maps of the local degree of order $\eta(\boldsymbol{r})$ at steady state under irradiation with large dense cascade ($b=4002$, density $=80\%$, $T=0.09$ eV, system size 64^3) at increasing disordering frequency: (a) $\Gamma_b=1\ s^{-1}$; (b) $\Gamma_b=10\ s^{-1}$; (c) $\Gamma_b=100\ s^{-1}$. White corresponds to fully ordered and black to fully disordered sites. Note the small isolated antiphase domains in (a), and the newly created cascade in the lower right corner of (b).

ordered zone ($t\approx 0.04$ s here), an unusual microstructure may develop, comprised of well-ordered domains whose sizes, however, remain finite. Such a microstructure is indeed observed in the following section.

B. Steady states under sustained irradiation

We now turn to the steady states that are stabilized by sustained irradiation with dense cascades. To ensure that the system has reached steady state, simulation times are run long enough so that initially fully disordered and fully ordered states give statistically identical results. For large cascade sizes, three distinct steady states are identified by direct visualization of the configurations, as illustrated in Fig. 2. At low flux [Fig. 2(a)], the alloy remains long-range ordered, i.e., there is only one macroscopic variant, which may however contain small isolated antiphase domains. At high flux [Fig. 2(c)], the system is mostly disordered, although it may possess some short-range order. At intermediate flux [Fig. 2(b)], there is a new state in the sense that the alloy is locally well ordered, but all four variants are present in domains of finite size. This state thus corresponds to a patterning of the order parameter. The presence of the four variants is further confirmed by displaying *B* atoms with a color code (see Fig. 5 in Ref. 29). For small cascade sizes, and in particular in the limiting case where $b=1$, no patterning of order can be detected at steady state.

C. Dynamical phase boundaries and phase diagram

We now construct the boundaries delimiting the domains of stability of the steady states identified in Sec. III B. There are two kinds of boundaries: from LRO to a non-LRO state, i.e., either to the state of patterning of order or to the disordered state, and from the patterning state to the disordered state.

The transition from the LRO phase to a non-LRO phase is determined using the standard method of inspection of the structure factor intensity, $I(\mathbf{k})$, at the superlattice positions, $\mathbf{k}=\mathbf{k}^*$.[27] This intensity scales with the system size in the LRO phase, while in the patterning and disordered states it is independent of the system size (see an example in Fig. 6 in Ref. 29). Alternatively, the transition can also be determined

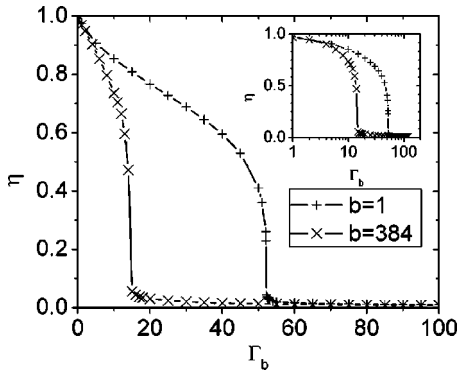

FIG. 3. Global order parameter η vs Γ_b for $b=1$, and $b=384$. System size is 128^3. The inset is the same data in semilog plot. Both transitions are of first order, but for $b=1$, the discontinuity is small. Lines are only guides for the eye.

by counting the number of *B* atoms that belong to each of the four translation variants: the LRO phase contains one, and only one, macroscopic cluster. In the absence of LRO, the *B* atoms are evenly distributed among the four variants. This second approach yields transition frequencies identical to those determined by monitoring the superlattice intensity.

Alternatively, the transition from the LRO to a non-LRO state can be determined by measuring the steady-state degree of order η as a function of the ballistic jump frequency. In the absence of irradiation, the transition is clearly of first order (not shown here), with a discontinuity from $\eta=0$ to $\eta=0.66$ at the transition temperature $T=0.155$ eV. In the presence of ballistic jumps, for all cascade sizes studied here, the order parameter displays a clear discontinuity at the transition $\Gamma_b=\Gamma_{b,c}$, and this transition is thus of first order (see Fig 3). For $b=1$, the discontinuity is smaller, as seen in Fig. 3, and the transition is weakly of first order.

We now turn to the boundary between the patterning state and the disordered state. The identification of this boundary is not straightforward, as the disordered state evolves continuously into the patterning state. As Γ_b is reduced so as to drive the alloy from disordered steady states to patterned steady states, we did not observe any discontinuity of the superlattice structure factor, either in intensity or in shape. The patterning state could in fact be described as a macroscopically disordered phase with order fluctuations that are abnormally coherent, intense, and long-lived. We propose here to define the state of patterning of order from the characteristics of the spatial fluctuations of order.

There is no exact theory that can describe the behavior of fluctuations near an equilibrium first-order transition, and *a fortiori* near a nonequilibrium first-order transition. Far from the transition, however, fluctuation-dissipation relationships provide us with quantitative expressions for pair correlation functions. While these expressions have been first derived using mean-field approximations, a general derivation can be obtained once it is assumed that there exists a grand potential for the system at hand.[31] For a binary alloy, a configuration is fully determined by the knowledge of the occupation function for the *B* species on all lattice sites, and one defines the thermodynamic average of this function on site *n* as c_n. The Helmhotz free-energy functional *F* is decomposed as $F=F_0$

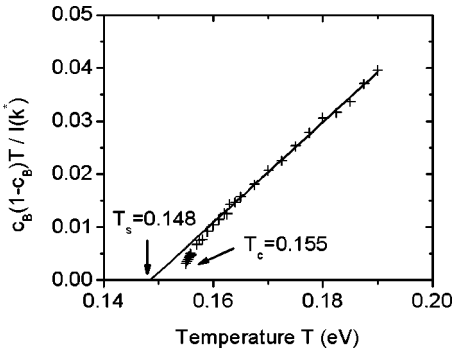

FIG. 4. $c_B(1-c_B)T/I(k^*)$ vs T for equilibrium transition (system size 64^3). k^* is the superlattice diffraction peak for $L1_2$ structure.

$+\Phi$, where $F_0=\beta^{-1}\Sigma_n[c_n \ln c_n+(1-c_n)\ln(1-c_n)]$ is the ideal solution contribution to F—or the noninteracting part of F, and Φ is interacting part, which contains all many-body-type interactions, including all entropy contributions beyond the point entropy. Taking advantage of a fluctuation-dissipation relationship, the Fourier transform of the Warren-Cowley pair correlation function, $\alpha(\mathbf{k})$, in the disordered state, is related to Φ through

$$\alpha(\mathbf{k}) = \frac{k_B T}{k_B T - c_B(1-c_B)S^{(2)}(\mathbf{k},T)}, \tag{1}$$

where $S^{(2)}(\mathbf{k},T)$ is the Fourier transform of $\partial^2\Phi/\partial c_i \partial c_j$. The latter matrix is simply the stability matrix with respect to concentration fluctuations. We now restrict our discussion to $\mathbf{k}=\mathbf{k}^*$. In the high temperature limit, $S^{(2)}(\mathbf{k}^*,T)$ reaches a constant value $S^{(2)}(\mathbf{k}^*)$. The high-temperature regime of Eq. (1) predicts therefore that $\alpha(\mathbf{k})$ should diverge at $k_B T_s = c_B(1-c_B)S^{(2)}(\mathbf{k}^*)$, and T_s is commonly referred to as the ordering instability temperature. In our Monte Carlo simulations, we can directly measure $\alpha(\mathbf{k})$ since, by definition, it is related to the structure factor of a configuration $I(\mathbf{k})$, through $\alpha(\mathbf{k})=I(\mathbf{k})/c_B(1-c_B)$. As first proposed by Cook,[32] though within a mean-field context, a plot of $c_B(1-c_B)T/I(\mathbf{k}^*)$ vs T should yield a linear regime with slope unity at high temperature, and the intercept of this linear regime with the temperature axis defines T_s. This linear regime is indeed observed experimentally[33] and in computer simulations[34] for alloys at thermodynamic equilibrium.

We first validate this method on our alloy system by restricting ourselves to equilibrium situations ($\Gamma_b=0$), at temperatures above the order-disorder transition temperature. As seen in Fig. 4, a linear regime is clearly identified at high temperature, and the slope, 0.94 ± 0.01, is in very good agreement with the predicted value. The instability temperature determined from the linear extrapolation is $T_s=0.149$ eV. Upon approaching the transition temperature, one observes in the plot Fig. 4 a downward curvature, which is due to heterophase fluctuations, and $I(\mathbf{k}^*)$ diverges at $T_c=0.155$ eV. The fact that $T_c>T_s$ is typical of first-order transition, whereas $T_c=T_s$ is expected for a second-order transition. The ratio T_s/T_c takes a value of 0.961, in excellent agreement with the value of 0.962 obtained by Chen and Cohen for the $A1$-$L1_2$ transition in Cu_3Au.[33]

In a mean-field approximation with pairwise atomic interactions, Eq. (1) reduces to the well-known Krivoglaz-Clapp-Moss (KCM) formula,[28,35] as $S^{(2)}(\mathbf{k},T)=V(\mathbf{k})$, the Fourier transform of the pairwise atomic interactions. In this approximation, the linear regime identified at high temperatures in a plot such as Fig. 4 should extend all the way down to the transition temperature, and the mean-field interpretation of T_s is that it is the temperature at which the disordered alloy becomes unstable with respect to long-range ordering. While the terminology of ordering instability is widely spread, one should be aware that, in Monte Carlo simulations, no transition from a nucleation and growth regime to a spinodal ordering regime has been observed upon crossing the $T=T_s$ value.[22,34,36] We stress, however, that here we define T_s from the high temperature regime, and therefore it is not restricted by a mean-field approximation.

We return to the case of an alloy under irradiation, for which we would like to analyze the fluctuations of order in a way similar to Eq. (1) and Fig. 4. In 1984, Martin[37] showed that, in a mean-field approximation and in the absence of any cascade effect, the steady-state concentration profile reached under irradiation is equivalent to the one reached at equilibrium, albeit at a higher effective temperature $T_{\text{eff}}=T(1+\Gamma_b/\langle\Gamma_{\text{th}}\rangle)$, where $\langle\Gamma_{\text{th}}\rangle$ is an average atomic jump frequency for thermally activated jumps.[38] Vaks and co-workers[39,40] generalized this result by deriving an effective KCM formula, both for decomposition and ordering transformations. This effective KCM relationship is simply the equilibrium one evaluated at the effective temperature, T_{eff}. An alternative way of studying order fluctuations under irradiation relies on the use of the stochastic mean-field potential that governs dynamical phase stability.[41–43] Assuming the existence of a nonequilibrium fluctuation-dissipation relationship, the second derivative of this potential with respect to the order parameter, evaluated in the disordered phase, yields a direct measure of the fluctuations at $\mathbf{k}=\mathbf{k}^*$. A straightforward calculation of this derivative for the $A1$-$L1_2$ stochastic potential[43] indicates again that the fluctuations are identical to the ones of an equilibrium system evaluated at the effective temperature, T_{eff}.

We thus propose to analyze order fluctuations under irradiation by assuming that, at $\mathbf{k}=\mathbf{k}^*$, Eq. (1) still provides a valid framework if evaluated at the effective temperature, T_{eff}. Under irradiation, transitions between steady states can be induced by varying the temperature or the ballistic jump frequency, Γ_b. We consider the case where the irradiation temperature is held constant, as in the present simulations. Replacing T by T_{eff} in Eq. (1), in the large Γ_b limit, one now defines the ballistic frequency for ordering instability, $\Gamma_{b,s}$

$$\frac{c_B(1-c_B)(\Gamma_b+\langle\Gamma_{th}\rangle)}{I(\mathbf{k}^*)} = \Gamma_b - \Gamma_{b,s}. \tag{2}$$

From the KMC simulation data, in order to perform a plot of $c_B(1-c_B)(\Gamma_b+\langle\Gamma_{\text{th}}\rangle)/I(\mathbf{k}^*)$ vs Γ_b, one needs to determine $\langle\Gamma_{\text{th}}\rangle$. A self-consistent use of the effective temperature criterion would use the value of $\langle\Gamma_{\text{th}}\rangle$ in the fully disordered state, which can be analytically calculated and takes the value $\langle\Gamma_{\text{th}}\rangle_d \approx 499\ \text{s}^{-1}$ for the present irradiation temperature. This

value agrees very well with the one obtained from KMC simulations, $\langle\Gamma_{th}\rangle_{d,KMC}\approx 505\ s^{-1}$, by calculating the vacancy diffusion coefficient in an alloy irradiated at a very high ballistic frequency, $\Gamma_b=500$. Inserting these values into Eq. (2) leads to linear plots, but not with a slope unity. The origin of this failure resides in the fact that, near the transition, the short-range order present in the alloy suppresses significantly the thermally activated migration of the vacancy, through higher activation energies and correlated jumps. As $\Gamma_b/\langle\Gamma_{th}\rangle$ represents a measure of the relative forcing intensity of the alloy, ignoring the effect of the SRO on $\langle\Gamma_{th}\rangle$ results in an underestimation of the relative forcing intensity. Measurements of vacancy diffusion coefficients in the disordered phase near the transition reveal that $\langle\Gamma_{th}\rangle$ varies very slowly with Γ_b. The simplest correction is thus to assume that, for each cascade size b, $\langle\Gamma_{th}\rangle$ takes a constant value that reflects the effect of SRO on the vacancy migration. For $b=1$, for instance, an average value of $\langle\Gamma_{th}\rangle_{b=1,KMC}\approx 277\ s^{-1}$ is measured for $70\ s^{-1}\leqslant\Gamma_b\leqslant 120\ s^{-1}$. If we now use this value to build the plot suggested by Eq. (2), a linear regime is found, with a slope 1.02. For practical reasons, instead of relying on the $\langle\Gamma_{th}\rangle$ values measured through vacancy diffusion coefficients, which have error bars of several percent, we let $\langle\Gamma_{th}\rangle$ be a fitting parameter so that the slope of the linear regime is 1. For $b=1$, for instance, this modified procedure leads to $\langle\Gamma_{th}\rangle_{b=1,fit}=267\ s^{-1}$, and a well-defined linear regime is obtained, as seen in Fig. 5. The ordering instability ballistic frequency in this case is determined to be $\Gamma_{b,s}=47.8\ s^{-1}$. Similarly to the equilibrium case, a downward curvature is observed just above $\Gamma_{b,c}$, and the behavior is typical of classical first-order transitions.

We now turn to the case of large cascade size. The expected linear behavior is still observed for large Γ_b values, as seen in Figs. 6 and 7. The behavior near the transition frequency, however, differs from the one observed for the thermal case or for $b=1$. An upward curvature is clearly visible upon approaching the transition, and the ordering instability frequency determined by the extrapolation of the linear fit, $\Gamma_{b,s}$, is now greater than the transition frequency, $\Gamma_{b,c}$. We propose to define the state of patterning of order as the regime where $\Gamma_{b,c}<\Gamma_b<\Gamma_{b,s}$. The interpretation of the unusual inequality $\Gamma_{b,c}<\Gamma_{b,s}$ is that, in this interval of ballistic frequencies, the high-Γ_b behavior predicts that the alloy should be unstable towards ordering, but complex atomic correlations have prevented the stabilization of the LRO phase, stabilizing instead a state with strong and persistent fluctuations of order. This picture is consistent with our direct observations of the dynamical stabilization of well-ordered domains that do not coarsen, as seen in Fig. 2(b).

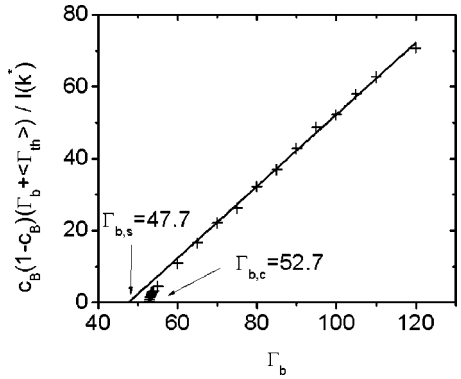

FIG. 5. $c_B(1-c_B)(\Gamma_b+\langle\Gamma_{th}\rangle)/I(k^*)$ vs Γ_b for $b=1$ (system size 64^3). k^* is the superlattice diffraction peak for $L1_2$ structure. $\langle\Gamma_{th}\rangle$ is an average thermal atomic jump frequency.

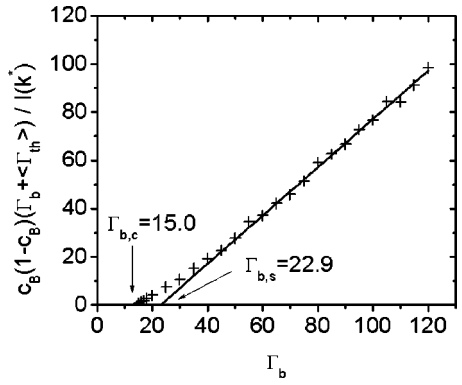

FIG. 6. $c_B(1-c_B)(\Gamma_b+\langle\Gamma_{th}\rangle)/I(k^*)$ vs Γ_b for $b=384$ (system size 64^3). k^* is the superlattice diffraction peak for $L1_2$ structure. $\langle\Gamma_{th}\rangle$ is an average thermal atomic jump frequency (see the text for definition). Note that $\Gamma_{b,c}$ is smaller than $\Gamma_{b,s}$.

This above analysis of the KMC results is used to build a dynamical phase diagram (see Fig. 8). This diagram displays three noticeable features.

(i) There is a minimum cascade size for the patterning of order to be possible. This threshold value is around $b=100$.

(ii) The patterning-disorder boundary does not depend strongly on the cascade size. It only shifts from $\Gamma_{b,s}=47.8$ for $b=1$ to $\Gamma_{b,s}=17.9$ for $b=4002$.

(iii) The LRO-patterning boundary, for low-flux values, approaches a power-law behavior with an exponent ≈ -1.5.

IV. KMC RESULTS AND ANALYSIS FOR NONSTOICHIOMETRIC ALLOYS

In Sec. III we have shown that, when the cascade size exceeds a threshold value, patterns of chemical order can

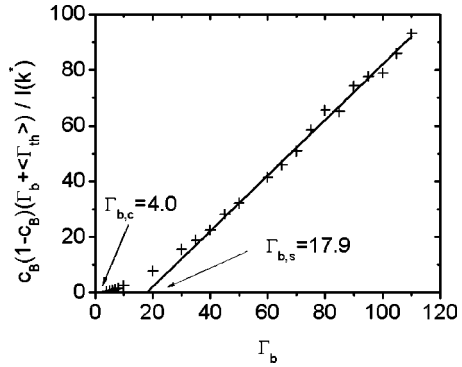

FIG. 7. $c_B(1-c_B)(\Gamma_b+\langle\Gamma_{th}\rangle)/I(k^*)$ vs Γ_b for $b=4002$ (system size 64^3). k^* is the superlattice diffraction peak for $L1_2$ structure. $\langle\Gamma_{th}\rangle$ is an average thermal atomic jump frequency (see the text for definition). Note that $\Gamma_{b,c}$ is smaller than $\Gamma_{b,s}$.

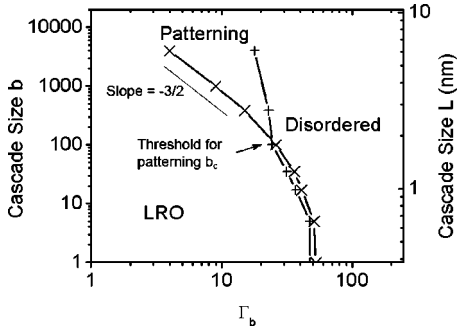

FIG. 8. Dynamical phase diagram ($T=0.09$ eV). The threshold for patterning of order is $b \approx 100$. For a given b, the cascade size L is obtained using Ni_3Al atomic density.

spontaneously form in a stoichiometric alloy, i.e., for $c_B = 25\%$. Similar patterning should also be possible in nonstoichiometric alloys. In addition, nonstoichiometric alloys may also undergo compositional patterning, as composition and chemical order are coupled by thermodynamics and kinetics.[44] We consider here two compositions, with 23% and 12% B atoms. The latter composition lies inside the equilibrium two-phase field at $T=0.09$ eV, while the former composition lies within the single-phase $L1_2$ field. In both cases, we anticipate that the excess A atoms will segregate at the antiphase boundaries, leading to inhomogeneities of the composition field. Patterning of order is still analyzed with the generalized fluctuation-dissipation approach using Eq. (3), while we study compositional patterning by monitoring the structure factor centered around $\mathbf{k}=\mathbf{0}$: a peak for a nonzero wave vector is the signature of compositional patterning.[26]

A. Alloy with $c_B = 0.23$

All the simulations for this alloy are run with a 128^3 system in order to increase the **k**-space resolution for the analysis of the structure factor. For large cascade size, $b=4002$ in Fig. 9, a distinctive peak is found near the Bragg peak, for Γ_b values ranging between 2 and 50 s^{-1}. This peak, which attests to the presence of a characteristic length scale for composition heterogeneities, disappears between $\Gamma_b = 50$ s^{-1} and $\Gamma_b = 60$ s^{-1}.

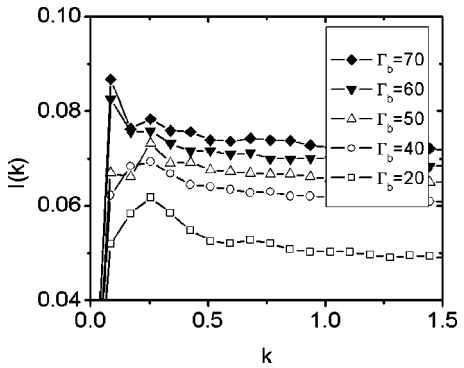

FIG. 9. Structure factor $I(k)$ spherically averaged around the Bragg peak $\mathbf{k}=\mathbf{0}$ at steady state for $c_B=0.23$ with $b=4002$ (system size 128^3).

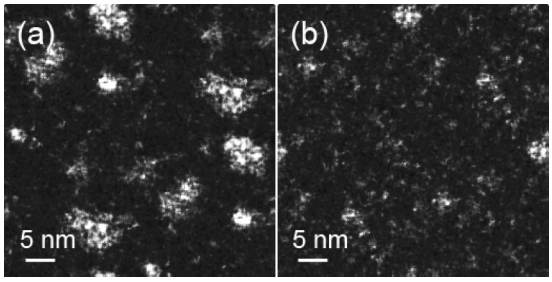

FIG. 10. Maps of the square of the local degree of order, $\eta(\mathbf{r})^2$ (averaged over 30 fcc cells) at steady state for $c_B=0.12$ with $b=4002$: (a) $\Gamma_b=0.05$; (b) $\Gamma_b=0.1$. System size is 128^3.

For the same cascade size $b=4002$, the patterning-disorder boundary, determined by plotting $c_B(1-c_B)(\Gamma_b + \langle\Gamma_{th}\rangle)/I(\mathbf{k}^*)$ vs Γ_b (see Fig. 7 in Ref. 29), is located at $\Gamma_{b,s}=13.4$ s^{-1}, while the LRO-patterning transition takes place at $\Gamma_{b,c}=2$ s^{-1}. Note that in the plot used to determine $\Gamma_{b,s}$ the KMC data remain above the linear regime for ballistic frequencies up to $\Gamma_b \approx 40$ s^{-1}. We thus conclude that compositional patterning and patterning of order take place over a similar range of ballistic jump frequencies. Similar results and conclusion were obtained for $b=384$.

For small cascade size, e.g., $b=5$, no peak could be detected near the Bragg position (see Fig. 8 in Ref. 29), even for a ballistic jump frequency $\Gamma_b=37$ s^{-1}, i.e., just above the order-disorder transition boundary, $\Gamma_{b,c}=36.0$ s^{-1}. We conclude that compositional patterning does not take place for $b=5$. Patterning of order was not observed either for $c_B = 0.25$, in agreement with the results reported in Sec. III. Similar results and conclusion were reached for $c_B=0.23$ and $b=35$.

B. Alloy with $c_B = 0.12$

Figure 10 shows maps of the chemical order parameter in an alloy with $c_B=0.12$ under sustained irradiation with $b=4002$, which corresponds to a cascade size of 6 nm. This particular composition has been chosen because it is close to the compositions used in the experimental works of Nelson *et al.*[45] and Schmitz *et al.*[46] The map of η^2, rather than η, is shown for more direct comparison with dark-field transmission electron microscopy images. Several finite-size ordered domains are present, regardless of the initial state. The large majority of these precipitates consists of a single variant. The precipitate size is around 6–10 nm with $\Gamma_b=0.05$ s^{-1}, and 3–5 nm with $\Gamma_b=0.1$ s^{-1}. Composition maps (not shown here) indicate that the ordered precipitates are significantly enriched in B species, with compositions close to 25%. For $\Gamma_b=0.05$ s^{-1}, the structure factor near the Bragg peak displays a clear maximum at small k values, which constitutes an additional proof of compositional patterning. In this regime, the resulting microstructure is thus comprised of B-rich ordered domains, embedded in a disordered matrix that is depleted in B species. For $\Gamma_b=0.1$ s^{-1}, this maximum in $I(\mathbf{k})$ near the Bragg peak is not always observed in the configurations explored at steady state, indicating that, at this Γ_b value, the system is close to the transition between the patterning and the disordered states.

V. DISCUSSION

We first discuss the case of stoichiometric alloys. For dense and large cascades, KMC simulations indicate that irradiation can stabilize a steady-state microstructure comprised of well-ordered domains of finite size. This patterning of order is rationalized by following the annealing of the disordered zone produced by one cascade in a long-range ordered matrix. This annealing proceeds in two stages: first the formation of new ordered domains in the initially disordered zone, and second the elimination of these domains by migration of their APBs. If the characteristic time for cascade initiation is between the characteristic times for these two stages, the initially long-range ordered matrix is destabilized by the repeated introduction of new ordered domains, leading to an equal proportion of all order variants, four in the case of the $L1_2$ structure. Yet, on a local scale, the alloy is well ordered because the cascade frequency is not high enough to destroy the chemical order.

A key ingredient in the dynamical stabilization of patterns of order is the formation of new ordered domains in the disordered zone created by the cascade. If the cascade is too small or too dilute, the presence of the long-range ordered matrix prevents new domains from nucleating, thus making it impossible to stabilize patterns of order. The kinetic parameters of an alloy may also influence this first stage, as they dictate the path of the vacancy, and thus the kinetics of formation of stable ordered domains in a disordered matrix. In general, however, vacancy migration energy is smaller in a disordered phase than in an ordered one, and this favors the transient formation of new domains. KMC simulations were performed for the same alloy considered in this work, except using a different set of kinetic parameters, where $\varepsilon_{AA}^{(1)}=\varepsilon_{BB}^{(1)}$ and $\varepsilon_{AV}^{(1)}=\varepsilon_{BV}^{(1)}$. Two-stage annealing of disordered zones and patterning of order were observed for that alloy as well.

It is somewhat remarkable that this two-stage reordering has not yet been reported in the literature, to the best of our knowledge. In fact, using KMC simulations where thermally activated jumps proceed by direct exchange of atoms, Abromeit and Matsumura[21] explicitly reported that no new ordered domains formed upon annealing of cascade-induced disordered zones in an $L1_2$ structure. We believe that this difference must be due to the fact that the cascades modeled in that work were too dilute or too small. In the limiting case where the disordered zones are very large and dense, one should always observe the formation of antiphase domains, regardless of the mechanism responsible for atom migration. Two additional relevant elements should be mentioned. First, once a cascade has formed, vacancies are predominantly found inside the cascade core, whereas interstitials are found at the periphery of the cascade.[19] Second, according to the MD simulations reviewed in the Introduction, the disordered zones produced by cascades, while lacking long-range order, exhibit significant short-range order. These two effects, which were not included in the present simulations, should favor the formation of new ordered domains.

Direct visualization of the configurations only allows for a qualitative assessment of the presence of patterns of order. Here, we propose a quantitative approach based on the analysis of the spatial fluctuations of order, by evaluating a fluctuation-dissipation relation at an effective temperature. It is interesting to note that the concept of an effective temperature has been proposed in other driven systems, e.g., for "jammed" granular systems.[47,48] We note, however, that, in case of irradiation with finite relocation range,[6,39] the concept of an effective temperature becomes questionable, as T_{eff} would be a function of the wave vector $\mathbf{k}$. It is then more appropriate to use the concept of effective interactions. We have not tested whether T_{eff}, which is here only considered at $\mathbf{k}=\mathbf{k}^*$, is indeed independent of $\mathbf{k}$. We also note that other methods may exist to identify the state of patterning of order, for instance by analyzing the temporal fluctuations of the order parameter. These points are left for future work.

The main results of this work are best summarized in a dynamical phase diagram (see Fig. 8). As the cascade size increases, the domain of stability of the patterned state becomes larger. This trend can be simply understood by considering the effect of the cascade size on the characteristic time scales of the two-stage reordering process. Once b is larger than the size of a stable ordered nucleus, the cascade size no longer plays a significant role in the first stage, and the boundary between patterned and disordered states should be almost independent of b. This expectation is in good agreement with our quantitative analysis. The boundary between patterned and LRO states, however, should display a clear b dependence, since, for a fixed volume of disorder initially introduced, the time for the annealing of antiphase domains increases with their size, in agreement with the classical Allen-Cahn kinetics. In the companion paper, we show analytically that, in the limit of large cascade sizes, the LRO-patterned state boundary should follow a power law with a $-3/2$ exponent.[7] This analytical result is in excellent agreement with the present KMC results. The dynamical phase diagram also indicates that there exists a minimum cascade size for patterning of order to become possible. This threshold value, here $b\approx 100$, is not an absolute value *per se*, and it should depend significantly on several parameters. The rationalization offered here suggests in particular that the threshold size will increase when temperature increases, or when the cascade density decreases.

In the limiting case $b=1$, no patterning is ever observed in the simulations, and the order-disorder transition has become a weak first-order one. We note that within the framework of the Landau theory, the $A1$-$L1_2$ transition cannot be of second order, as the third Landau-Lifshitz requirement is not satisfied.[49]

We are not aware of any experimental observations of patterning of order that would directly correspond to the KMC results presented here. Ni_3Al and Cu_3Au alloys would be good candidates for such studies, and various TEM techniques could be used to image the ordered domains. Following the analysis developed in this work, x-ray or neutron diffuse scattering experiments could be used for a quantitative assessment of patterning of order, by recording the intensity of the structure factor at the superlattice positions at steady state for various irradiation fluxes or for various irradiation temperatures. In the present KMC simulations, the vacancy concentration is fixed, independently of the ballistic jump frequency. In analyzing experiments, however, one would have to take into account the enhancement of the ther-

mally activated atomic mobility under irradiation by the supersaturation of point defects.

A generalization of the present results offers a simple rationalization for puzzling experimental results reported for the Ni_4Mo alloy under irradiation. Ni_4Mo displays the remarkable property of possessing two competing ordered states with different symmetry, commonly referred to as the LRO and SRO states. Under irradiation with 1 MeV electrons, i.e., in the absence of displacement cascades, only one ordered phase is found at steady state.[50] Under ion irradiation, however, there exists a temperature range where the LRO and SRO states coexist dynamically at steady state.[51] By extending the present KMC results to the Ni_4Mo alloy, it is expected that the disordered zones produced by displacement cascades during ion irradiation would first reorder according to the SRO symmetry, as is observed during thermal annealing of a completely disordered state.[52] For intermediate rate of introduction of cascades, one would then expect the stabilization of patterns of coexisting LRO and SRO states. More experimental work is required, though, to determine the spatial distribution of the two ordered states when they coexist dynamically.

We now turn to nonstoichiometric alloys. Patterning of order, combined with segregation or wetting at APBs, leads to compositional patterning, even for alloy compositions inside the equilibrium $L1_2$ field ($c_B=23\%$). For dilute alloys ($c_B=12\%$), patterning of order leads to formation of small ordered precipitates embedded in a disordered matrix. This kind of microstructure is in fact very similar to the ones reported by Nelson *et al.*[45] and by Schmitz *et al.*[46] in Ni-irradiated Ni–Al alloys with Al concentrations of 11.5% and 12%, respectively. In these works, patterning of order could potentially have been induced indirectly by a compositional patterning.[27] This alternative explanation, however, is less convincing since the maximum characteristic scale of the patterns would then be bounded by $4\pi R_c$,[6] which translates into 3.6 nm for Ag–Cu.[53] On the other hand, when patterning of order is directly induced by cascade zone reordering, the size of ordered domains is bounded by the cascade size, which can extend up to 10 nm.[19] Additional experimental work is required to characterize these microstructures at the nanoscale.

It is interesting to stress the similarities between the present results and our previous work on the effect of the forced atomic relocation range in displacement cascade.[6,26,27,53] As mentioned in the Introduction, this range, as it exceeds a critical value, can directly lead to compositional patterning, and indirectly to patterning of order when one of the two phases involved in the decomposition displays an ordering tendency. The effect of the cascade size identified in the present work is complementary to that of the relocation range, in the sense that it can directly induce patterning of order, and indirectly compositional patterning in nonstoichiometric alloys. In both cases, the relevant length scale has to exceed a critical value for patterning to become possible. In both cases, stable steady-state patterns emerge continuously from a disordered and homogeneous state, until reaching a maximum scale, where the alloy undergo a discontinuous dynamical transition to a phase that possesses long-range order. We also note that in both cases the indirect effects are brought about by the thermodynamic coupling of the composition field and of the chemical order field. We were able to rationalize compositional patterning induced by relocation range by showing analytically that the forced mixing introduces effective long-range repulsive interactions between species, which were competing with the physical short-range attractive interactions. At least from a qualitative perspective, we can here again invoke a similar concept for patterning of order. The present patterns of order share similarities with long period structures and incommensurate phases, which are commonly reproduced by using competing interactions with different ranges. A formal mathematical treatment to derive these effective interactions in the case of patterning of order, however, is currently lacking.

Several simplifications have been used in the present KMC simulations. First, interstitials have been ignored, whereas they could contribute to disordering, through random recombination,[54] or to reordering, in particular at low temperature.[55] Although these contributions would add complexity, it appears that they would not affect the main result that patterning of order becomes possible when cascades are large and dense. Second, vacancies are treated as conservative species, with a fixed vacancy concentration. The use of a fixed vacancy concentration is motivated by the fact that point defects reach their steady-state concentration much faster than the chemical order. As we use an *a priori* imposed vacancy concentration, the time scale and the fluxes given in the simulations cannot be directly compared to experimental values. For comparison with these values, the time scale should be rescaled by the actual point defect concentration under irradiation, which can be estimated using rate equations.[1,37] The absence of sources and sinks for point defects implies that there are no net chemical fluxes in our simulation cells. It is well documented that these fluxes, combined with the irreversibility of the point defect elimination reaction, can induce compositional patterning, and, as a consequence, patterning of order in alloy systems with ordering tendency.[56] The microstructure of such patterns, however, is directly linked to that of the sinks. For the moderately elevated temperatures considered here, the sink separation distance should thus be at least an order of magnitude larger than the scale predicted in the present simulations. The confirmation of the mechanism identified in this work for patterning of order thus requires a combined analysis of the patterns of order and of the microstructure of the irradiated material. Finally, stress effects were not considered in the simulations. As elastic interactions are long range, they are susceptible to alter the scale of patterns of order. One way to minimize elastic interactions is to choose an alloy for which the $A1$ and $L1_2$ phases are lattice matched, e.g., the nimonic PE 16 superalloy.

Finally, we propose that irradiation-induced patterning of order could be used for the synthesis of functional nanocomposites. In particular, the extension of the present results to the Fe–Pt and Co–Pt alloy systems suggests that nanocomposites comprised of $L1_0$ and disordered phases could be obtained by processing alloys with $c_{Pt}\approx 30\%$ to 40% under carefully chosen irradiation conditions. These conditions would be such that they retain the $L1_0$ phase, which has a high ordering energy in these systems, but would disorder

the $L1_2$ phase. Nanocomposites of $L1_0$ FePt or CoPt, which are hard magnetic phases, and of $A1$, a soft magnetic phase, have been proposed as very good candidates for exchange-spring magnets, producing permanent magnets with enhanced energy products.[57–59]

VI. CONCLUSION

We used kinetic Monte Carlo simulations to study the effect of the size of disordered zones produced by displacement cascades on the steady states stabilized in an $L1_2$ ordered alloy under irradiation. We observed that one large and dense disordered zone reorders following a two-stage process, involving first the transient formation of small and new ordered domains, followed by the shrinkage of these domains to the benefit of the matrix. Under sustained irradiation conditions, for large enough disordered zones, three steady states are found. In addition to the expected long-range ordered state and disordered state, a state of patterning of order is identified. A dynamical phase diagram is constructed, which yields the domain of stability of these three states. The boundary between the patterned and the disordered states is determined from the structure of the fluctuations of order, by using a fluctuation-dissipation relationship evaluated at an effective temperature. While the present work offers rationalization for some experimental results on Ni_4Mo and Ni–Al alloys, systematic experiments are suggested to test the present predictions. It is also suggested that irradiation-induced patterning of order could be used to synthesize functional nanocomposites, in particular, exchange-spring magnets.

ACKNOWLEDGMENTS

Stimulating discussions with R. S. Averback, D. D. Johnson, Jiwen Liu, and Jin-Min Zuo are gratefully acknowledged. This material is based upon work partly supported by the U.S. Department of Energy, Division of Materials Sciences under Award No. DEFG02-91ER45439, through the Frederick Seitz Materials Research Laboratory at the University of Illinois at Urbana-Champaign, by the Materials Computation Center at the University of Illinois, National Science Foundation, under Grants DMR 99-76550 and DMR 03-25939, and by the University of Illinois Campus Research Board. We also thank the FS-MRL Center For Computation for its assistance.

*Email address: bellon@uiuc.edu

[1] G. Martin and P. Bellon, Solid State Phys. **50**, 189 (1997).
[2] G. Nicolis and I. Progogine, *Self-organization in Nonequilibrium Systems: From Dissipative Structures to Order Through Fluctuations* (Wiley, New York, 1977).
[3] M. C. Cross and P. C. Hohenberg, Rev. Mod. Phys. **65**, 851 (1993).
[4] W. Jäger and H. Trinkhaus, J. Nucl. Mater. **205**, 394 (1993).
[5] N. M. Ghoniem, D. Walgraef, and S. J. Zinkle, J. Comput.-Aided Mater. Des. **8**, 1 (2002).
[6] R. Enrique and P. Bellon, Phys. Rev. Lett. **84**, 2885 (2000).
[7] J. Ye and P. Bellon, following paper, Phys. Rev. B **70**, 094105 (2004).
[8] M. L. Jenkins and C. A. English, J. Nucl. Mater. **108–109**, 46 (1982).
[9] M. L. Jenkins, K.-H. Katerbau, M. Wilkens, Philos. Mag. **34**, 1141 (1976).
[10] M. L. Jenkins and M. Wilkens, Philos. Mag. **34**, 1155 (1976).
[11] S. Muller, M. L. Jenkins, C. Abromeit, and H. Wollenberger, Philos. Mag. A **75**, 1625 (1997).
[12] L. M. Howe and M. H. Rainville, Philos. Mag. A **39**, 195 (1979).
[13] A. Laupheimer and M. Wilkens, Phys. Status Solidi A **55**, 497 (1979).
[14] T. Diaz de la Rubia, A. Caro, and M. Spaczer, Phys. Rev. B **47**, 11 483 (1993).
[15] M. Spaczer, A. Caro, M. Victoria, and T. Diaz de la Rubia, Phys. Rev. B **50**, 13 204 (1994).
[16] F. Gao and D. J. Bacon, Philos. Mag. A **71**, 43 (1995).
[17] F. Gao and D. J. Bacon, Philos. Mag. A **71**, 65 (1995).
[18] N. V. Doan and R. Vascon, Nucl. Instrum. Methods Phys. Res. B **135**, 207 (1998).
[19] R. S. Averback and T. Diaz de la Rubia, Solid State Phys. **51**, 281 (1998).
[20] P. Bellon, Y. Grandjean, M. Przybylowicz, F. Soisson, and G. Martin, Nucl. Instrum. Methods Phys. Res. B **102**, 72 (1995).
[21] C. Abromeit and S. Matsumura, Philos. Mag. A **82**, 2287 (2002).
[22] T. A. Abinandanan, F. Haider, and G. Martin, Acta Mater. **46**, 4243 (1998).
[23] C. Frontera, E. Vives, T. Castán, and A. Planes, Phys. Rev. B **55**, 212 (1997).
[24] M. Athenes, P. Bellon, G. Martin, and F. Haider, Acta Mater. **44**, 4739 (1996).
[25] R. Enrique and P. Bellon, Phys. Rev. B **60**, 14 649 (1999).
[26] R. Enrique and P. Bellon, Phys. Rev. B **63**, 134111 (2001).
[27] J. Liu and P. Bellon, Phys. Rev. B **66**, 020303(R) (2002).
[28] M. Krivoglaz, *Theory of X-ray and Thermal-Neutron Scattering by Real Crystals* (Plenum, New York, 1969).
[29] See EPAPS Document No. E-PRBMDO-70-036429 for supplementary results. A direct link to this document may be found in the online articles HTML reference section. This document may also be reached via the EPAPS homepage (http://www.aip.org/pubservs/epaps.html) or from ftp.aip.org in the directory/epaps/. See the EPAPS homepage for more information.
[30] S. M. Allen and J. W. Cahn, Acta Metall. **27**, 1085 (1979).
[31] D. D. Johnson, F. J. Pinski, and J. B. Staunton, in *Methods in Materials Research* (Wiley, New York, 2000), Unit 2b.3.
[32] H. E. Cook, Mater. Sci. Eng. **25**, 127 (1976).
[33] H. Chen and J. B. Cohen, Acta Metall. **27**, 603 (1979).
[34] B. Chakraborty and Z. Xi, Phys. Rev. B **53**, 5063 (1996).
[35] P. C. Clapp and S. C. Moss, Phys. Rev. **142**, 418 (1966).
[36] C. Billotet and K. Binder, Z. Phys. B **32**, 195 (1979).
[37] G. Martin, Phys. Rev. B **30**, 1424 (1984).
[38] Note that here Γ_b is defined as the frequency per atom of ballistic exchanges between pairs of atoms, and therefore, for consis-

tency, $\langle \Gamma_{th} \rangle$ is half the average frequency for the thermally activated migration of one atom.
[39] V. Vaks and V. Kamyshenko, Phys. Lett. A **177**, 269 (1993).
[40] V. Vaks and S. V. Beiden, Phys. Lett. A **182**, 140 (1994).
[41] P. Bellon and G. Martin, Phys. Rev. B **38**, 2570 (1988).
[42] P. Bellon and G. Martin, Phys. Rev. B **39**, 2403 (1989).
[43] F. Haider, P. Bellon, and G. Martin, Phys. Rev. B **42**, 8274 (1990).
[44] P. Bellon and G. Martin, Phys. Rev. B **66**, 184208 (2002).
[45] R. S. Nelson, J. A. Hudson, and D. J. Mazey, J. Nucl. Mater. **44**, 318 (1972).
[46] G. Schmitz, J.C. Evert, F. Hardsmeier, M. Urhmacher, and F. Haider, Phys. Rev. B **63**, 224113 (2001).
[47] L. Berthier and J-L. Barrat, Phys. Rev. Lett. **89**, 095702 (2002).
[48] I.K. Ono, C.S. O'Hern, D.J. Durian, S.A. Langer, A.J. Liu, and S.R. Nagel, Phys. Rev. Lett. **89**, 095703 (2002).
[49] F. Ducastelle, *Order and Phase Stability in Alloys* (North-Holland, Amsterdam, 1991).
[50] S. Banerjee, K. Urban, and M. Wilkens, Acta Metall. **32**, 234 (1984).
[51] P. Bellon, P. R. Okamoto, and G. Schumacher, J. Nucl. Mater. **205**, 438 (1993).
[52] J. Mayer and K. Urban, Acta Metall. **33**, 539 (1985).
[53] R. Enrique, K. Nordlund, R. S. Averback, and P. Bellon, J. Appl. Phys. **93**, 2917 (2003).
[54] T. Mukai, C. Kinoshita, and S. Kitajima, Philos. Mag. A **47**, 255 (1983).
[55] C. Abromeit, H. Wollenberger, S. Matsumura, and C. Kinoshita, J. Nucl. Mater. **276**, 104 (2000).
[56] K. C. Russel, Prog. Mater. Sci. **28**, 229 (1984).
[57] R. Skomski and J. M. D. Coey, Phys. Rev. B **48**, 15812 (1993).
[58] E. F. Kneller and R. Hawig, IEEE Trans. Magn. **27**, 3588 (1991).
[59] J. P. Liu, C. P. Luo, Y. Liu, and D. J. Sellmyer, Appl. Phys. Lett. **72**, 483 (1998).